The Impact of Anodization on the Thermal Performance of Passively Cooled Electronic Enclosures Made of Die-cast Aluminum

Zhongchen Zhang [1], Michael Collins [2], Chris Botting [3], Eric Lau [3], Majid Bahrami [1] *
[1] Laboratory for Alternative Energy Conversion, School of Mechatronic Systems Engineering, Simon Fraser University, Surrey, British Columbia, Canada
[2] Solar Thermal Research Laboratory, Department of Mechanical and Mechatronics Engineering, University of Waterloo, Waterloo, Ontario, Canada
[3] Delta-Q Technologies, Burnaby, British Columbia, Canada
* Corresponding author – email: mbahrami@sfu.ca

Abstract

Natural convection and thermal radiation from anodized die-cast aluminum enclosures designed for the application of high power density battery chargers are investigated experimentally. Several sample enclosures are prepared using the two most commonly available types of anodization: i) Type II-black; and ii) Type III-clear. The enclosures are then tested in a customized natural convection - thermal radiation test chamber. Total emittance of bare and anodized surface is measured using Fourier Transform Infrared Reflectometer (FTIR) spectroscopy. The results show that the total hemispherical emissivity of die-cast aluminum sample surface can be significantly improved from 0.14 to 0.92 after anodizing. More importantly, anodization can lead to a considerable reduction in thermal resistance (up to 14.7%) compared to the identical untreated enclosures. Because of the unique surface morphology of anodized die-cast aluminum, it is also observed that the same improvement of thermal emissivity as well as overall thermal performance can be achieved by either types of anodization.

Keywords

Thermal radiation, Natural Convection, Anodization, Electronic cooling.

Nomenclature

A	Surface area [m^2]
C_p	Specific heat at constant pressure [$J/(kg \cdot K)$]
C_3	Third radiation constant [$\mu m \cdot K$]
E	Surface radiative emissive power [W/m^2]
F	View factor
H	Enclosure height [m]
h	Convective heat transfer coefficient [$W/(m^2 \cdot K)$]
I	Current [A]
k	Thermal conductivity [$W/(m \cdot K)$]
L	Enclosure length [m]
Q	Heat transfer rate [W]
R	Thermal resistance [°C/W]
s	Standard deviation
T	Temperature [°C]
V	Voltage [V]
W	Enclosure width [m]

Greek Symbol

σ	Stefan-Boltzmann constant [$W/m^2 \cdot K^4$]
ε	Thermal emissivity
δ	Absolute uncertainty
λ	Wavelength [μm]

Subscript

b	Black body
c	Convective heat loss
r	Radiative heat loss
h	Heat sink
∞	Ambient environment

1. Introduction

Reliable thermal management of electronic devices is always crucial, and of great importance, especially in power electronic industry, where the cooling loads are ever-increasing. Active cooling technologies, on the basis of force convection, are most widely used because of their relatively higher cooling capacity. However, active cooling require parasitic power, can be noisy (e.g., fan, pump) and poses a risk of device overheat and malfunction induced in case of the failure. Passive cooling technologies work based on natural convection and thermal radiation, and offer a reliable alternative cooling solution with no additional moving part and zero parasitic power consumption, which is desirable in electronic cooling applications, when applicable.

In theory, convective heat transfer can be calculated by Newton's Law of cooling as Eq. (1):

$$Q_c = hA(T_h - T_\infty) \quad (1)$$

Where, h is the convective heat transfer coefficient, A is the heat transfer surface area, and T_h , T_∞ are the average surface and ambient temperature, respectively. Meanwhile, the modified Stefan-Boltzmann equation [1] can be used to calculate radiative heat exchange from a surface to the ambient:

$$Q_r = AF\sigma\varepsilon(T_h^4 - T_\infty^4) \quad (2)$$

where, F is the view factor from surface to surrounding, σ is the Stefan-Boltzmann constant [5.67×10^{-8} $W/m^2 \cdot K^4$] and ε is the surface thermal emissivity, respectively. Numerous studies were focused on the enhancement of natural convection by investigating different geometries. Studies by Ahmadi et al. [2] [3] are good examples illustrating the natural heat transfer improvement by introducing the interrupted fins. However, radiative heat transfer is overlooked in the majority of the

Table 1. Literature review on the radiative heat transfer from finned enclosures

Ref.	Approaches	Fin Geometry	Material	Surface Treatment	Surface Emissivity	Emissivity Measuring Method	Qr/Q(%)
Chaddock et. al [4]	Experimental	Cylindrical	Extruded Aluminum	-	0.99	-	33
				Polished	-	-	10 - 20
Sparrow et. al [5]	Experimental Analytical	Pin	Extruded Aluminum	Black Anodizing	0.82	Gier-Dunkle heated-cavity reflectometer.	25 - 45
Rao et. al [6]	Experimental Numerical	Rectangular	Extruded Aluminum	Black Board Paint	0.85	-	25 - 40
Rao et. al [7]	Numerical	Rectangular	Extruded Aluminum	-	0.85	-	36 - 50
Yu et. al [8]	Experimental Analytical	Rectangular	Pure Aluminum	Black Anodizing	0.80	-	27
Tamayol et. al [9]	Experimental Analytical	Rectangular	Extruded Aluminum	-	0.75	-	50

existing studies and is given less consideration for manufacturing the naturally-cooled heat sinks. Nevertheless, more evidence is emerging that radiation play a critical role in passively cooled devices. One of the pioneering studies on this topic was conducted by Edwards et al. [4]. They reported that the contribution of radiation heat transfer was one third of the total heat dissipation from an extended cylindrical surface. Following studies further affirm that great portions of heat loss in passive cooled devices are contributed by radiation regardless of its external geometry [4] to [9]. Table 1 provides an overview of the pertinent literatures that support the important role of thermal radiation in the passive cooled systems.

In radiative heat transfer, surface area, view factor from enclosure to ambient, and surface thermal emissivity are the three major parameters when the temperature difference is fixed, as it can be seen in Eq. (2). The surface area and view factor are all associated with heat sink geometry, which are often limited by the actual product design. The surface emissivity, as a surface radiative property, often can be improved by several surface finishing techniques. Thus, this study focuses on the heat transfer enhancement enabled by the thermal emissivity improvement.

The majority of heat sinks used in the industry are made of aluminum alloys, either from extrusion, casting, or machining process. Several methods are often used to improve the thermal emissivity of aluminum surfaces, such as abrasive blasting, spray painting, anodizing. Of all the techniques, anodizing is the most efficient and cost-effective method. Known as a process of growing an anodic layer integrated with the surface of aluminum alloys in an electrolytic bath, it is usually adopted to enhance aesthetic appeal, along with wear and corrosion resistance to the original part in many applications. According to the US Military specification [MIL-A-8625F] [10], anodic coating for aluminum and its alloys are categorized into 3 types and 2 classes. Due to the environmental concerns, Type I [Chromic acid anodizing] is only used in rare cases while Type II [Sulfuric acid anodizing] and Type III [Hard anodic coatings] are the mostly common and well-adopted techniques. Attribute to the porous structure of the anodic layer, the dyes and pigments can be readily absorbed and sealed in the small pores and result in various colorful appearance, also referred as class I, or colored anodizing. Subsequently, class II is the clear anodizing with original look of the anodic layer itself.

In general, most of previous studies either solely emphasized on the experimental and modeling work of thermal radiation in naturally cooled heat sinks as listed in Table 1 or investigated the influence of the key parameters in anodizing process. These parameters have an important impact on the morphology of the anodic layer, which will in turn affect the total emittance of treated surface as shown in [11] [12] [13]. To the best of the authors' knowledge, conjugate analysis involving both aspects has not been investigated thoroughly in the literature. We also noticed that no study has placed their focus on the thermal emissivity of anodized die-cast aluminum. This could be due to the limited availability of the material. Therefore, in this study, die-cast aluminum battery charger enclosures [Delta-Q Technologies] are anodized in Type II-black and Type III-clear, by a local metal surface treatment company [Spectral Finishing]. The overall thermal performance of three types of heat sink with different surface finishes is tested and analyzed. The thermal emissivity of the tested heat sinks is also measured and reported.

2. Experimental Approach

2.1 Sample Preparation

Several unprocessed enclosures were prepared and cleaned in advance for anodizing and testing, as shown in Fig. 1. All samples were made from die-cast process using aluminum A380 alloy. The length [L], width [W] and height [H] of the enclosures were 23cm, 17cm and 7.5cm, respectively. Isopropyl alcohol solution was used to remove dusts and stains from the enclosure surface before anodizing.

This electrochemical reaction occurred in a 15% sulfuric acid bath with special additives at 14℃ to achieve a 25μm thick anodic layer for both Type II and Type III. Because of the high content of impurities in this type of die-cast aluminum alloys, increasing the thickness of anodic layer any further is of great difficulty. In Type II-Black anodizing, the black dyes were added into the electrolyte bath to reach the desired dark black finish that absorbed through capillary effect. Finally, the cold nickel fluoride method was applied to accomplish proper sealing. Two sample enclosures were prepared for each type of anodization to ensure repeatability of the testing results. The detailed numbers of sample preparation are provided in Table 2.

Table 2. Number of samples prepared with various surface finish

Amount of samples	Bare	Type-II Black	Type-III Clear	Type-III no sealing
Enclosures	2	2	2	-
Plates	2	2	2	2

Additionally, eight flat plate samples $[2.5\text{cm} \times 5.0\text{cm}]$ were prepared with the same material, cleaned and anodized with the same procedures for thermal emissivity measurements.

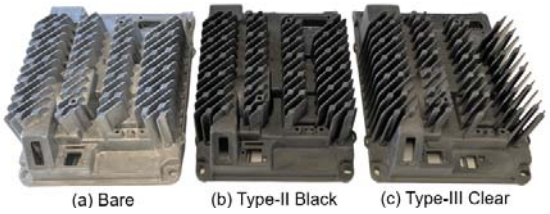

Figure 1. Delta-Q battery charger enclosures, samples made using die-cast process, aluminum A380 alloy; (a) before and after various types of anodization (b) and (c).

2.2 Test Procedure

Figure 2 shows the schematic of our experimental setup. A customized natural convection - thermal radiation test chamber was built with 4 mm thick acrylic plastic $[k = 0.2\text{W}/(\text{m} \cdot \text{K}), \rho = 1180\text{kg}/\text{m}^3, C_p = 1470\text{J}/(\text{kg} \cdot \text{K}), \varepsilon = 0.9]$. The length, width, and height of the chamber were 50 cm [2.2 x L], 50 cm [3.0 x W] and 50 cm [6.6 x H] of the tested enclosure to minimize the influence of chamber walls on the internal natural convection airflow. This chamber was built to reduce the impact of the air disturbance from surroundings as well as to improve the result consistency from various tests.

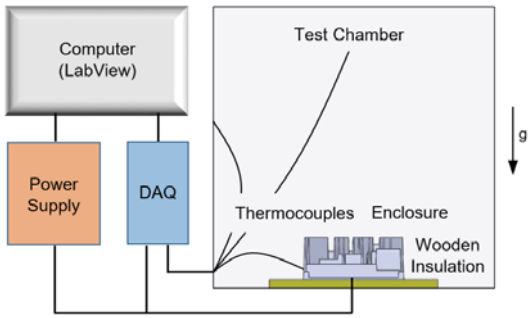

Figure. 2: Schematic diagram of experimental setup.

The sample battery charger enclosures were tested in the horizontal orientation. A centimeter-thick wooden plate was placed underneath the enclosure to provide thermal insulation from the base. The ports and gaps on the enclosure were taped with adhesive aluminum foils to ensure airtight sealing, preventing the potential thermal leakage by air convection from the internal regions. Five ultra-thin polyimide film heaters with pressure sensitive adhesive of three different sizes of 1.3cm×5.1cm [0.5in×2.0in], 2.5cm×2.5cm [1.0in×1.0in] and 2.5cm×5.1cm [1.0in×2.0in] were attached to the back of the enclosure to mimic the heat generation from diodes, transistors, inductors, transformers and other heat generating components. All heaters had a power density of $1.6\text{W}/\text{cm}^2$ $[10\text{W}/\text{in}^2]$ and were driven by a programmable AC/DC power supply. Fourteen T-type copper-constantan thermocouples with uncertainty of $\pm 0.5℃$ were installed using aluminum foil tapes at various positions to monitor the temperature distribution along the enclosure base, chamber inner ambient and chamber wall. The location of the thermocouples and heating components is indicated in Fig.3. A NI9213 [National Instruments] data acquisition module was used to record the temperature readings from the thermocouples and a NI9229 [National Instruments] for monitoring the voltage and current through the heater to calculate the actual supplied power.

The tests were run in an open lab environment facing north, free of direct sunlight from the windows. The room temperature was kept constant at $22℃$. Each enclosure was tested with various power levels ranging from 20W to 80W. Steady-state condition was reached when the partial derivative of all temperatures with respect to time - except the ambient - was within $0.001℃$ for $30\,\text{mins}$. This was considered as the thermal equilibrium on the interfaces of the tested enclosures and chamber walls, i.e., the summation of convective and radiative heat transfer leaving each interface became equal to the heat input into the battery charger.

The thermal emissivity of each anodized surface was measured using Fourier Transform Infrared Reflectometer [FTIR] spectroscopy [400T, Surface Optics Corporation] at room temperature, where the measured range of the wavelength of infrared is from $2.5\mu\text{m}$ to $25\mu\text{m}$. The spectral hemispherical emissivity and total hemispherical emissivity of sample plates were determined in the same ambient condition. The micro structures of anodic layer were imaged by a field mission scanning electron microscopy [Nova NanoSEM, Thermo Fisher Scientific]. All samples were coated with 10nm iridium using a high vacuum sputter system [EM ACE 600, Leica Microsystems] before SEM imaging.

3. Results and discussions

3.1 Thermal emissivity of anodized surface

Emissivity as a surface radiative property specifies the radiative capability of a real surface as compared with emission from a black body at the same temperature. In general, it depends on two factors, the temperature and direction. The emissivity value - that is widely accepted and reported in most textbooks - is the total hemispherical emissivity. This value should be averaged over all the wavelengths and the directions. However, most data are only available for a limited range of wavelength and directions due to the constrains of measurement and the interests of research, i.e., emissivity over mid- and long-infrared [MWIR, LWIR] is important in thermal applications. Additionally, it can also be spectral. The Wien's Displacement Law [1] expresses the spectral distribution of a black body with the corresponding wavelength to temperature as Eq. (3):

$$\lambda_{max} \cdot T = C_3 \tag{3}$$

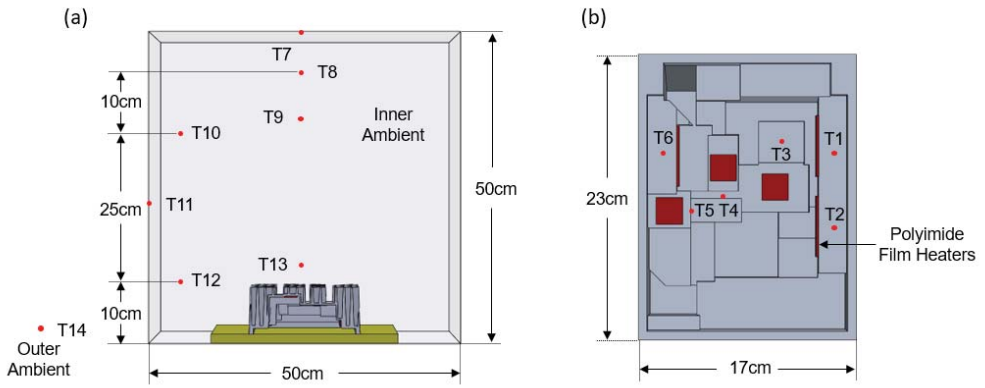

Figure 3. Schematic of thermocouples locations and heat generating components in (a) test chamber (b) battery charger enclosure.

where, the λ_{max} is the peak wavelength and C_3 is the third radiation constant, $2898\mu m \cdot K$, respectively. According to Eq. (3), the maximum spectral emissive power is shifting towards shorter wavelength as temperature increases. For a blackbody at 100℃ [373.16K], the peak emission occurs over $7.8\mu m$ and great portion of the emitted radiation fall into the range of mid-infrared [MWIR]. It further ascertains that most of the radiation from electronic cooling applications could be found within this range. Ideally, it would be preferable to keep the sample at certain temperature to simulate the real working environment during the measurement. However, conditioning the ambient environment of the spectrometer is challenging.

Figure 4 (a) shows the spectral hemispherical emissivity of various samples at wavelengths from $2.5\mu m$ to $25\mu m$. The spectral emissivity justifies the radiation ability of measured surface to the black body at each wavelength at the same temperature, and shows as Eq. (4):

$$\varepsilon_\lambda(\lambda, T) = \frac{E_\lambda(\lambda, T)}{E_{\lambda b}(\lambda, T)} \tag{4}$$

where, E is emissive power and subscript λ, b denote spectral emissive power from measured surface and a black body, respectively. Surprisingly, the spectral emissivity of a bare die-cast aluminum surface is very selective and has the rising trend towards the short wavelength. It can reach 0.4 at wavelength of $2.5\mu m$ while drops to 0.1 at $25\mu m$. This varying properties of bare die-cast aluminum may imply the potential enhancement of thermal radiation in operational scenarios with high temperature. As for anodized surfaces, the emissivity over the entire measured spectrums fluctuates within the range of 0.85 to 1. This significant improvement of emissivity can be gained by either types of anodization. Figure 4(b) shows the results for total hemispherical emissivity which are the quotient between the integration of spectral emissivity over the wavelength of $2.5\mu m$ to $25\mu m$ and the total emissive power of a black body at the same temperature. The following formulation [1] can be used to calculate total emissivity:

$$\varepsilon(T) = \frac{\int_{\lambda=2.5}^{\lambda=25} \varepsilon_\lambda(\lambda, T) E_{\lambda b}(\lambda, T) d\lambda}{\sigma T^4} \tag{5}$$

The error bars shown in Fig. 4(b) are comprised of the inaccuracy of the spectrometer [1%] and the standard deviation between different samples. The following can be observed from Fig. 4(b):

- The total emissivity of the type II-Black treated surface can reach 0.92 and it is improved nearly seven times compared to its original surface condition;
- The total emittance of both type II-Black and type III-Clear are nearly identical. This indicate that the black dyes may have limited contribution in terms of thermal emissivity improvement and may imply that the color of anodized surface not certainly reflect its own thermal emissive capability.

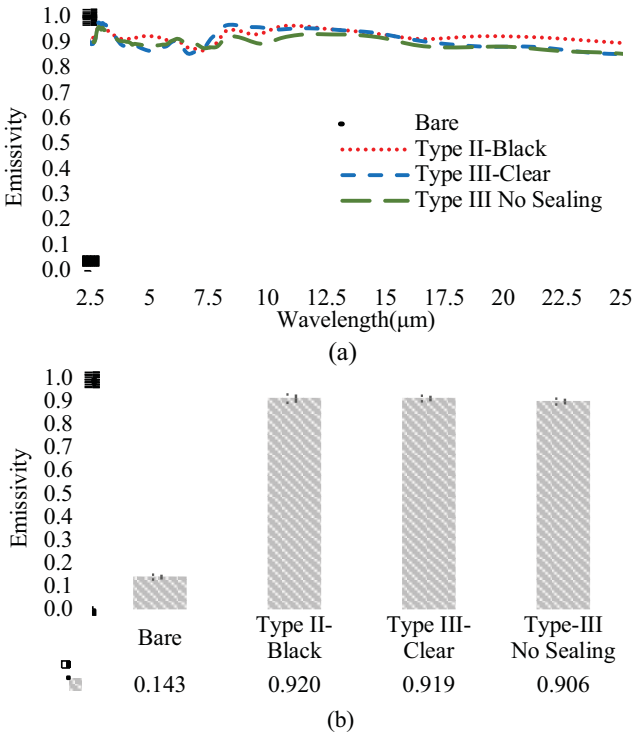

Figure. 4: (a) Spectral Hemispherical Emissivity (top) and (b) Total Hemispherical Emissivity (bottom) of Bare, anodized Type II-Black, Type III-Clear and no sealing sample.

In terms of the whole spectrum of light, the wavelength of electromagnetic radiation in the range of 390nm to 700nm is classified as visible light that is involved in the perception of different color in human eyes. Meanwhile, the infrared spectrum of thermal radiation is in the wavelength of 3μm to 15μm, the Mid-wavelength infrared to Long-wavelength infrared, which can be found usually within the application of power electronics and is of great interest in thermal radiation. It is noticeable 10x order of magnitude difference in the wavelength of spectrum distribution of visible light and infrared light that corresponding to the thermal radiation, which helps explaining the fact that colored surface offers the same thermal emissivity as un-dyed surface and the blackness of the surface is not necessarily associated to its emissive property within infrared region. It also reveals a possibility to maintain the same thermal improvement using type II anodization with colorful dyes to meet the various marketing needs. However, we still need to consider the thermal radiative properties of the dyes and its possible impact on the overall thermal emissivity, which require further investigation.

Figure 4 shows the influence of sealing on the thermal emissivity as well. Sealing is a process of precipitating an additional layer of sealants, seeing as a thin film, on top of the uncovered anodized surface to protect the pore structure and the dyes that are already absorbed inside. The easiest sealing method is called hydrothermal, which is applied by placing the parts in a hot water bath. Several other methods are also used to fulfill the same purposes. Among all, the cold nickel fluoride method is chosen by this anodizing vendor and it does help the total emittance increase slightly, i.e. from 0.906 to 0.919. Lee et al [12] have examined the effect of several sealing methods on the surface emissivity and concluded that the improvement after sealing, may attribute to the nature of the precipitated sealants in each method.

3.2 Surface morphology of anodic layers

Figure 5 shows the SEM images of the unsealed anodic layer which unveil the porous structure under the sealed film. The anodic layer consists of cells, in which each has a distinct boundary that separates it from others, shown in Fig. 5 (a). In addition to the unique hexagonally packed cells, Fig. 5 (c) displays a rather different surface structure, where the anodic films appear to be stacked layer-by-layer with small gaps and a few miniature pores scattering over the surface. With higher image magnification in Fig.5 (b) and (d), the details of two totally different morphologies provide a potential explanation for this phenomenon, namely, the density difference within the same die-cast aluminum sample. This commonly exists in the die-cast aluminum since the injection pressure of the molten metal may vary at different positions during the casting process. As such, the density of aluminum sample is unevenly distributed and porous textures are formed resulting in a layer-stacked structure resembling Fig. 4(c) and (d).

Unlike the porous anodic layer that formed on the surface of extruded aluminum alloys [12], the anodized surface of die-cast aluminum does not contain any individual pores aligned within the cells. The certain pattern of pores should be visible at higher magnification, but we fail to observe any arrangement that confirm its existence. Even with image magnification of 46,266× in Fig. 5(e), the surface structure remains as pore-less as stacked structures. This is mainly due to the composition of the aluminum alloys that is used in die-cast manufacturing, where the pure aluminum only takes up 80% to 90%. The rest of the constituents are mainly silicon, copper, zinc, other metallic elements and impurities from the manufacturing process. It is assumed that the existence of aforementioned contents interrupts the formation and growth of the anodic layer.

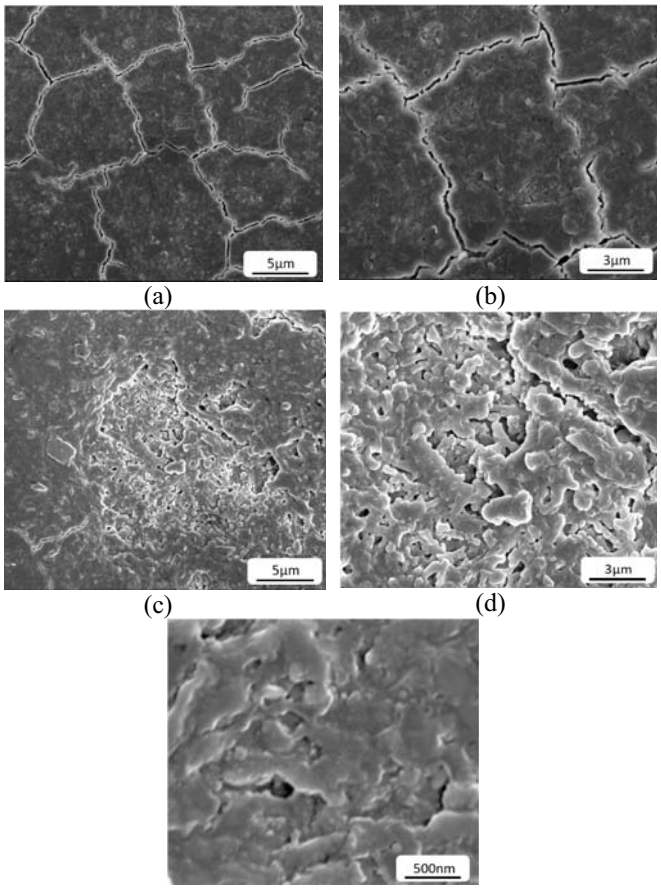

Figure. 5 SEM images of unsealed anodic layers of anodized die-cast aluminum. (a) and (b) show "hexagonally packed" cells; (c) and (d) indicate the porous and layer-stacked structure; (e) porous structure with higher magnification.

Figure 6 shows the surface morphology of sealed anodized surface after type II-Black and type III-Clear treatment. The boundaries or cracks that shape the cells are still partially visible from both images, which may be because of the relatively thin film from the sealing process. However, from the perspective of surface uniformity, the type III-Clear treated surface has comparatively high surface roughness compared to type II-black. This may lead to a potentially higher resistance to wear and corrosion. As a result of the pore-less and layer-stacked structure of anodized die-cast surface, the black dyes may have absorbed insufficiently within the anodic layer in type II-Black treatment as show in Fig. 6(a) as small stains that on the surface.

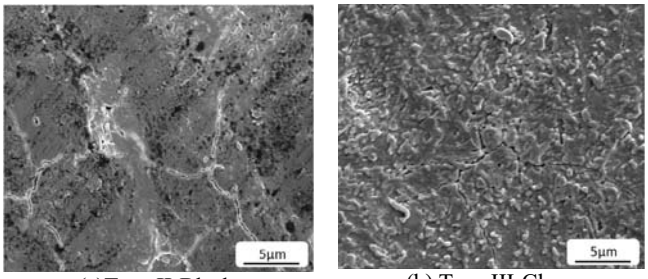

(a)Type II-Black (b) Type III-Clear

Figure. 6 SEM images of sealed anodic layer of (a) Type II-Black and (b) Type III-Clear. (a) the surface of type II-Black under scanning electron microscope where we assume most of dyes are rather visible and attached on the surface after sealing. It looks like stains on the surface. (b) shows the morphology of type III-Clear treatment and it appears to be a relatively rough surface.

Even though the micro surface morphology appears to be different after the sealing process, the emissivity measurement from previous sections reveals the same improvement for both types of anodization. Consequently, we may able to conclude that, the unique surface structure made by anodizing process, i.e. porous layer, has a fundamental impact on thermal emissivity, and that black dyes and sealing process are less important.

3.3 Thermal performance of anodized enclosure

The thermal test results are shown in Fig. 7, which are the average temperature difference between the enclosure base and the ambient temperature, and the total thermal resistance of the enclosure, including both natural convection and thermal radiation. The experimental uncertainty of temperature and power input measurements as well as standard deviation among each test and sample are shown as error bars in Fig.7. The horizontal error bars represent the calculated uncertainty from voltage and current measurements while the vertical uncertainty includes the calculated errors of temperature difference measurements and standard deviation from tests for the same sample. Since the maximum calculated uncertainty for temperature measurement is $\pm 4.7\%$, some error bars in Fig. 7 (a) are rather invisible. Uncertainty analysis are listed below.

$$\delta_{\Delta T} = \sqrt{(\delta_T)^2 + (\delta_T)^2} \tag{6}$$

$$\delta_{\Delta T \cdot s} = \sqrt{(\delta_{\Delta T})^2 + s^2} \tag{7}$$

$$\frac{\delta_{\dot{Q}}}{\dot{Q}} = \sqrt{\left(\frac{\delta_V}{V}\right)^2 + \left(\frac{\delta_I}{I}\right)^2} \tag{8}$$

$$\frac{\delta_R}{R} = \sqrt{\left(\frac{\delta_{\Delta T}}{\Delta T}\right)^2 + \left(\frac{\delta_{\dot{Q}}}{\dot{Q}}\right)^2} \tag{9}$$

$$\delta_{R \cdot s} = \sqrt{(\delta_R)^2 + s^2} \tag{10}$$

As shown in Fig. 7, anodization significantly improves the overall thermal performance of treated enclosures compared to the bare samples. In Fig. 7(a), the average base temperature drops around 6℃ on average, 12.2% in relative improvement, for an input thermal power of 80W. The average temperature of the base is also 3℃ lower [16.7% improved] even for a power input of 20W. The radiative heat transfer follows the surface temperature to the 4th power, Eq. (2). Indeed, for higher surface temperatures, the significance of thermal emissivity (and thermal radiation) will be more pronounced.

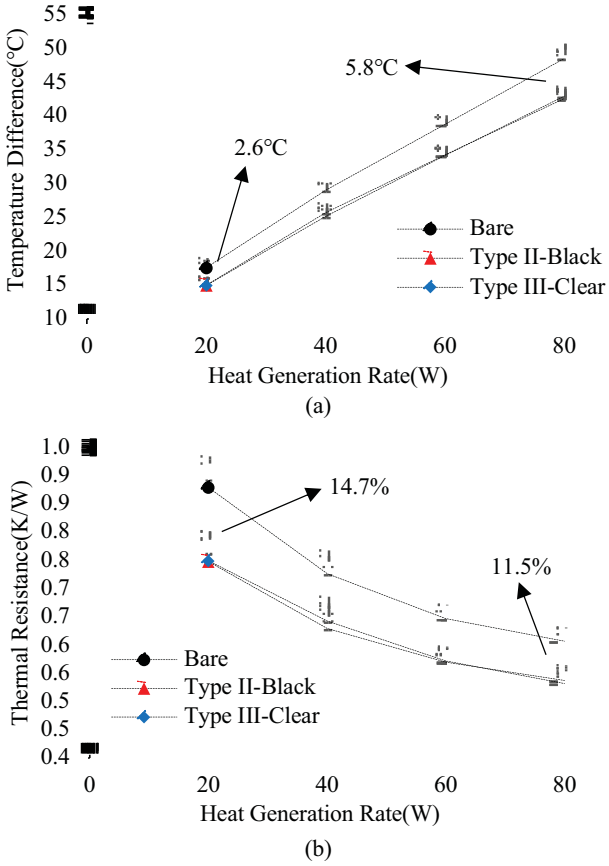

Figure. 7 (a) Average temperature difference between enclosure base and chamber ambient (b) Total thermal resistance (natural convection and thermal radiation) from tested enclosures.

The total thermal resistance of the enclosure can be improved up to 14.7% when after applying Type II-Black anodizing. The same enhancement was observed for Type III-Clear in our tests. This further confirms the significant impact of anodization on the overall thermal enhancement of die-cast aluminum enclosures.

4. Conclusions

A comprehensive experimental study was performed to investigate the impact of anodization on thermal radiation of naturally-cooled heat sinks. A number of die-cast aluminum enclosures were prepared and tested in our custom-designed testbed. The results indicated that the total emissivity of samples can be improved notably from 0.14 to 0.92 after using commercially-available anodizing treatments.

It was also shown that anodized die-cast aluminum naturally-cooled heat sinks perform significantly better, up to 15% reduction in overall thermal resistance, compared to the identical non-anodized enclosures. Due to the unique surface morphology of anodized die-cast aluminum, both types of anodization, Type II-Black and Type III-Clear, were able to provide the same enhancement in thermal radiation.

Acknowledgments

This research is supported by the funding from the Natural Sciences and Engineering Research Council of Canada (NSERC) Collaborative Research Development (Grant No. CRDPJ488777) and Delta-Q technologies. The author also would like to thank the 4D Labs of Simon Fraser University for their support.

References

[1]. Bergman, T. L., et al. "Fundamentals of heat and mass transfer", John Wiley & Sons Inc, USA (2011).

[2]. Ahmadi, M., Mostafavi, G. and Bahrami, M., "Natural convection from rectangular interrupted fins", International Journal of Thermal Sciences, 82, pp.62-71, 2014.

[3]. Ahmadi, M., Pakdaman, M.F. and Bahrami, M., "Pushing the limits of vertical naturally-cooled heatsinks", Calculations and design methodology, International Journal of Heat and Mass Transfer, 87, pp.11-23, 2015.

[4]. Edwards, J.A. and Chaddock, J.B., "An experimental investigation of the radiation and free convection heat transfer from a cylindrical disk extended surface", Trans. Am. Soc. Heat. Refrig. Air-Cond. Eng, 69, pp.313-322, 1963.

[5]. Sparrow, E.M. and Vemuri, S.B., "Natural convection /radiation heat transfer from highly populated pin fin arrays", Journal of heat transfer, 107(1), pp.190-197, 1985.

[6]. Rao, V.R. and Venkateshan, S.P., "Experimental study of free convection and radiation in horizontal fin arrays", International Journal of Heat and Mass Transfer, 39(4), pp.779-789, 1996.

[7]. Rao, V.D., Naidu, S.V., Rao, B.G. and Sharma, K.V., "Heat transfer from a horizontal fin array by natural convection and radiation—A conjugate analysis", International journal of heat and mass transfer, 49(19-20), pp.3379-3391, 2006.

[8]. Yu, S.H., Jang, D. and Lee, K.S., "Effect of radiation in a radial heat sink under natural convection", International Journal of Heat and Mass Transfer, 55(1-3), pp.505-509, 2012.

[9]. Tamayol, A., McGregor, F., Demian, E., Trandafir, E., Bowler, P., Rada, P. and Bahrami, M., January. "Assessment of thermal performance of electronic enclosures with rectangular fins: a passive thermal solution", In ASME 2011 Pacific Rim Technical Conference and Exhibition on Packaging and Integration of Electronic and Photonic Systems (pp. 269-276). American Society of Mechanical Engineers, 2011.

[10]. United Stated Military Specification No. MIL-A-8625F, 1993.

[11]. Le, H.G., Watcher, J.M. and Smith, C.A., "Comparison of sulfuric and oxalic acid anodizing for preparation of thermal control coatings for spacecraft", 1988

[12]. Lee, J., Kim, D., Choi, C.H. and Chung, W., "Nanoporous anodic alumina oxide layer and its sealing for the enhancement of radiative heat dissipation of aluminum alloy", Nano energy, 31, pp.504-513, 2017.

[13]. Kumar, C.S., Sharma, A.K., Mahendra, K.N. and Mayanna, S.M., "Studies on anodic oxide coating with low absorptance and high emittance on aluminum alloy 2024", Solar energy materials and solar cells, 60(1), pp.51-57, 2000.

[14]. Klampfl, B.F., "A parametric study of sulfuric acid anodized 5657 aluminum alloy coatings for thermal control applications", Doctoral dissertation, Rice University, 1998.